ISSN 1407-8880 TELECOMMUNICATIONS AND ELECTRONICS TELEKOMUNIKĀCIJAS UN ELEKTRONIKA 2008-8880

Initial Implementation of Generalized Haar-Like Orthonormal Transforms into FPGA-Based Devices - Part I: Signal Spectrum Analyzer-Synthesizer Module

Peteris Misans, Gatis Valters, Maris Terauds, Arturs Aboltins
Faculty of Electronics and Telecommunications, Riga Technical University,
Riga, LV-1010, Latvia, e-mail: *name.family@rtu.lv*

***Abstract*—This paper deals with the aspects of practical implementation of signal spectrum analyzer-synthesizer (SANSYN) and the basic notions for orthonormal parametrical Haar-like transform called "Rotation Angle Based Haar-like Transform" (RA-HT). The transform is very perspective for pulse-like signal processing. The presented RA-HT device is implemented as Altera's Cyclone II FPGA. A simplified block diagram and parameters of the SANSYN module are provided. The heart of the module is a two-sample CORDIC rotator. Three versions of the module are reviewed and the version comparison is provided. The versions differ by the number of rotators and speed. The version chosen for further development achieves the trade-off between the performance and the hardware consumption.**

***Index Terms*—CORDIC algorithm, FPGA, Generalization of Haar Functions, Parameterization of Orthogonal Transforms**

I. INTRODUCTION

GENERALIZATION of Haar functions presented in [1] supplements a rich collection of papers (approx. 300) issued by many authors (see [2]). Some notable references to the papers dealing with generalizations and applications of Haar functions reader can find in [1] and [3], but the most comprehensive list is in [2].

We suppose that the cornerstones of the description of discrete orthogonal (orthonormal) transforms are rotation angles of planes in Euclidian space [4]. The angular approach is very well known in linear algebra but it has not been used very often by signal processing people. It seems that H. C. Andrews [5] is a pioneer in the area of parameterization of fast orthogonal (orthonormal) transforms by rotation angles of planes. P. Rieder, together with colleagues, (for example, [6]) uses rotation angles in the context of CORDIC-based implementation of orthogonal wavelet transforms and DCT. The pioneer in introducing and using of rotation angle based orthogonal filters is P. P. Vaidyanathan [7]. We avoid here a detailed overview of all available works on rotation angle approach because of the limited space of the paper.

This paper continues description of the results obtained by "Phi-functions team" in the Riga Technical University. Simultaneously with theoretical studies we try to build up real FPGA-based devices [8]-[10] useful for signal processing. After the definition of subclasses of **R**otation **A**ngle Based **H**aar-like **T**ransform(s) (RA-HT) in [1] we presented the preliminary results of simulation of novel classes of RA-HT orthogonal filters in [11]. The aspects of practical implementation of the filters are highlighted in [12] submitted for this proceeding.

The present paper focuses on the implementation aspects of signal spectrum analyzer-synthesizer (SANSYN) module. Additionally, here are given the basic notions of RA-HT transforms that apply also to the second submitted paper – - [12]. We suppose also that the ideas exposed here and in [12] are novel.

II. BASICS

A. Basics of RA-HT Transform(s)

The RA-HT is one of the subclasses of **R**otation **A**ngles **B**ased **O**rthogonal **T**ransforms (RABOT) described in [4]. The RA-HT transform works akin to other well-known real orthogonal (orthonormal) transforms which for the fast calculation of spectrum (or signal synthesis) uses the product of sparse factorized matrices [11]:

$$\mathbf{Y} = \mathbf{\Phi}(\boldsymbol{\varphi}^{(n)}) \cdot \mathbf{X} = (\prod_{j=n}^{1} \mathbf{B}_{r\,j}) \cdot \mathbf{X},$$
$$\mathbf{Z} = \mathbf{X} = \mathbf{\Phi}^{T}(\boldsymbol{\varphi}^{(n)}) \cdot \mathbf{Y} = (\prod_{j=1}^{n} \mathbf{B}_{r\,j}) \cdot \mathbf{Y}, \quad (1)$$
$$\mathbf{B}_{r\,j} = \mathbf{B}_{r}(\varphi_j),\ \boldsymbol{\varphi}^{(n)} = [\varphi_1, ..., \varphi_j, ..., \varphi_n],$$
$$N = 2^n, \quad n = \log_2(N)$$

where $\mathbf{\Phi}$ is an orthogonal matrix with size N by N, but $\mathbf{X}$, $\mathbf{Z}$, and $\mathbf{Y}$ – input and two output column-vectors (real numbers), respectively. Each row of $\mathbf{\Phi}$ presents a single basis function (BF), but each element of $\mathbf{X}$ and $\mathbf{Y}$ can be treated as signal sample and spectrum coefficient, respectively. In the ideal case

the synthesized signal **Z**=**X**. The angle matrix $\boldsymbol{\varphi}^{(n)}$ has a specific structure (each next column has twice as less nonzero elements than previous) and contains *n* columns and *N/2* rows ($N = 8$ (n=3)):

$$\boldsymbol{\varphi}^{(3)} = \left[\boldsymbol{\varphi}_1 \;\; \boldsymbol{\varphi}_2 \;\; \boldsymbol{\varphi}_3\right]^T = \begin{bmatrix} \phi_{1\,1} & \phi_{2\,1} & \phi_{3\,1} & \phi_{4\,1} \\ \phi_{1\,2} & \phi_{2\,2} & 0 & 0 \\ \phi_{1\,3} & 0 & 0 & 0 \end{bmatrix}. \qquad (2)$$

The matrix $\mathbf{B}_{\mathrm{r}}$ is a **S**tairs-like **O**rthonormal **G**eneralized **R**otation **M**atrix $\mathbf{B}_{\mathbf{k}}$ (SOGRM – see [4]) with permutated rows. The permutation matrix is described more detailed in [1]. Briefly – the matrix $\mathbf{B}_{\mathrm{r}}$ has the structure with a SOGRM-like square sub-matrix in the left-upper corner and a unit matrix-like structure in the right-upper corner (see (3)). A common property of classical HT BFs and RA-HT BFs is the existence of segments with zero values for the same time intervals (argument). RA-HT BFs have multi-valued nonzero segments in the contrast to the classical HT BFs which are only two-valued in nonzero segments (see (4)).

B. Subclasses of RA-HT Transforms

[1] defines several subclasses of RA-HT transforms. The classification of RA-HTs is based on the limitations on the nonzero values of elements of angle matrix $\boldsymbol{\varphi}^{(n)}$. "In the case when the nonzero angles may have arbitrary values without limitations we are talking about RA-HT transform in general." - [11]. Here we omit detailed description of RA-HT transforms (see [1]) and provide information necessary only for the understanding of the topic.

Formula (3) shows factorized matrices $\boldsymbol{B}_{\mathrm{r}\ j}(\phi_j)$ for CRAIM-HT transform (one nonzero angle per matrix) when N=8:

$$\boldsymbol{\Phi}_8(\phi_1,\phi_2,\phi_3) = \mathbf{B}_{r\,3}\cdot\mathbf{B}_{r\,2}\cdot\mathbf{B}_{r\,1} = \begin{bmatrix} s_3 & c_3 & 0 & 0 & 0 & 0 & 0 & 0 \\ c_3 & -s_3 & 0 & 0 & 0 & 0 & 0 & 0 \\ 0 & 0 & 1 & 0 & 0 & 0 & 0 & 0 \\ 0 & 0 & 0 & 1 & 0 & 0 & 0 & 0 \\ 0 & 0 & 0 & 0 & 1 & 0 & 0 & 0 \\ 0 & 0 & 0 & 0 & 0 & 1 & 0 & 0 \\ 0 & 0 & 0 & 0 & 0 & 0 & 1 & 0 \\ 0 & 0 & 0 & 0 & 0 & 0 & 0 & 1 \end{bmatrix} \cdot \begin{bmatrix} s_2 & c_2 & 0 & 0 & 0 & 0 & 0 & 0 \\ 0 & 0 & s_2 & c_2 & 0 & 0 & 0 & 0 \\ c_2 & -s_2 & 0 & 0 & 0 & 0 & 0 & 0 \\ 0 & 0 & c_2 & -s_2 & 0 & 0 & 0 & 0 \\ 0 & 0 & 0 & 0 & 1 & 0 & 0 & 0 \\ 0 & 0 & 0 & 0 & 0 & 1 & 0 & 0 \\ 0 & 0 & 0 & 0 & 0 & 0 & 1 & 0 \\ 0 & 0 & 0 & 0 & 0 & 0 & 0 & 1 \end{bmatrix} \cdot \begin{bmatrix} s_1 & c_1 & 0 & 0 & 0 & 0 & 0 & 0 \\ 0 & 0 & s_1 & c_1 & 0 & 0 & 0 & 0 \\ 0 & 0 & 0 & 0 & s_1 & c_1 & 0 & 0 \\ 0 & 0 & 0 & 0 & 0 & 0 & s_1 & c_1 \\ c_1 & -s_1 & 0 & 0 & 0 & 0 & 0 & 0 \\ 0 & 0 & c_1 & -s_1 & 0 & 0 & 0 & 0 \\ 0 & 0 & 0 & 0 & c_1 & -s_1 & 0 & 0 \\ 0 & 0 & 0 & 0 & 0 & 0 & c_1 & -s_1 \end{bmatrix} \qquad (3)$$

where $s_j = sin(\phi_j)$, $c_j = cos(\phi_j)$.

The given table (TABLE I) summarizes brief definitions and examples for three subclasses of RA-HT. Basically, this table is taken from [11]. The present table is corrected and supplemented by examples.

Nonzero values of matrix $\boldsymbol{\Phi}$ elements are presented by the product of corresponding sine and cosine values, but the structure (not the elements!) of the matrix is identical to the Haar transform matrix for all subclasses of RA-HT transforms (see (4)).

For the simplest CRA-HT transform and N=8 (all nonzero angles are equal) we have:

$$\boldsymbol{\Phi}_8 = \begin{bmatrix} s^3 & s^2c & s^2c & c^2s & s^2c & c^2s & c^2s & c^3 \\ s^2c & c^2s & c^2s & c^3 & -s^3 & -s^2c & -s^2c & -c^2s \\ sc & c^2 & -s^2 & -sc & 0 & 0 & 0 & 0 \\ 0 & 0 & 0 & 0 & sc & c^2 & -s^2 & -sc \\ c & -s & 0 & 0 & 0 & 0 & 0 & 0 \\ 0 & 0 & c & -s & 0 & 0 & 0 & 0 \\ 0 & 0 & 0 & 0 & c & -s & 0 & 0 \\ 0 & 0 & 0 & 0 & 0 & 0 & c & -s \end{bmatrix}, \qquad (4)$$

but in the case when $\phi = \pi/4$ we obtain Haar transform matrix. From (4) we see that BFs with row indexes $p \le N/2$ are multi-valued in opposite to BFs with $p > N/2$, which are three-valued only.

TABLE I
SUMMARY OF THE SUBCLASSES OF RA-HT TRANSFORMS

Subclass	Restrictions for angles	Example (N=8, n=3)
Constant **R**otation **A**ngle HT (CRA-HT)	$\boldsymbol{\varphi}_j^{(n)} = [\overbrace{\phi, \phi, ..., \phi}^{N/(2^j)}, \underbrace{0, ..., 0}_{N/2}]^T$	$\boldsymbol{\varphi}^{(3)} = \begin{bmatrix} \pi/3 & \pi/3 & \pi/3 & \pi/3 \\ \pi/3 & \pi/3 & 0 & 0 \\ \pi/3 & 0 & 0 & 0 \end{bmatrix}^T$

Constant **R**otation **A**ngle **I**n **M**atrix (CRAIM-HT)	$\boldsymbol{\varphi}_j^{(n)} = [\overbrace{\phi_j, \phi_j, ..., \phi_j}^{N/(2^j)}, \underbrace{0, ..., 0}_{N/2}]^T$	$\boldsymbol{\varphi}^{(3)} = \begin{bmatrix} \pi/4 & \pi/4 & \pi/4 & \pi/4 \\ \pi/6 & \pi/6 & 0 & 0 \\ \pi/3 & 0 & 0 & 0 \end{bmatrix}^T$
HT with **R**educed **S**equences of Rotation **A**ngles (RSA-HT)	$\boldsymbol{\varphi}_j^{(n)} = [\overbrace{\phi_1, \phi_2, ..., \phi_{f(j)}}^{f(j)=N/(2^j)}, \underbrace{0, ..., 0}_{N/2}]^T$	$\boldsymbol{\varphi}^{(3)} = \begin{bmatrix} \pi/7 & \pi/3 & \pi/4 & \pi/5 \\ \pi/7 & \pi/3 & 0 & 0 \\ \pi/7 & 0 & 0 & 0 \end{bmatrix}^T$

C. Shapes and Properties of RA-HT Basis Functions

Each row of the transform matrix Φ represents a discrete BF. Here we can observe a rich diversity of shapes of BFs depending on the values of angles. In general, we may treat these functions as corrupted Haar functions (drawn with solid line in Fig. 1). On the other hand, we can treat described transforms as parametrical transforms in dependence on angles (parameters). The complexity of shapes of nonzero parts of BFs depends on the number and values of angles used for the building of transform. The invariance of nonzero part of shape of BF to shifting is a well-known property of HT and wavelets. This property is also true for CRA-HT and CRAIM-HT transforms but does not work in the case of RA-HT and RSA-HT transforms. That is, we can observe

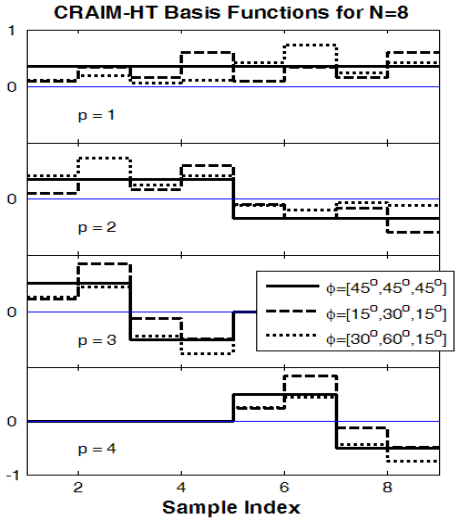

Fig. 1. Shapes of the first four discrete CRAIM-HT BFs for certain values of rotation angles and N=8

some similarity of CRA-HT and CRAIM-HT to orthogonal wavelets but we may not state that these functions are wavelets. Two differences are evident: each RA-HT BF contains a DC component, and BFs are not orthogonal to simple polynomials (vanishing moments). Are or are not the mentioned transforms members of wavelets or some generalized wavelets? We need a serious discussion on it with experts in the future.

D. RA-HT Basis Functions and Unit Sphere

The efficient geometrical comparison of different RA-HT transforms can be made by using a unit sphere (US) like in the case with CRAIMOT transforms [8]. If we change rotation angles for selected RA-HT transform in formula (1), the projections of ends of BF vectors of transforms create a certain picture on the surface of N-dimensional US. The density of the picture depends on the chosen transform, the number of angles used for the transform, and the step of angles (2° in figures below).

For example, for N=4 we have only four points on the US surface as a result of Haar BF vector end projections. In Fig. 2 we see that these projections for the simplest CRA-HT transforms draw only a few curve-like lines, and the coverage of sphere is very weak. Most areas are never covered ("white holes/patches"). That is because only one angle has been used for the change (selection or definition) of CRA-HT transform (see TABLE I). If we compare the CRA-HT trace with the trace of CRAOT from [8], we observe some similarity, but the coverage in the case of CRA-HT is poorer. The same applies to similarities between CRAIM-HT and CRAIMOT [8].

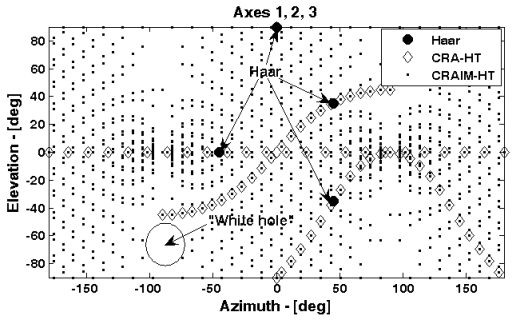

Fig. 2. Traces of CRAIM-HT and CRA-HT BFs vector end projections on the spread of surface of one of the unit sphere 3D projections

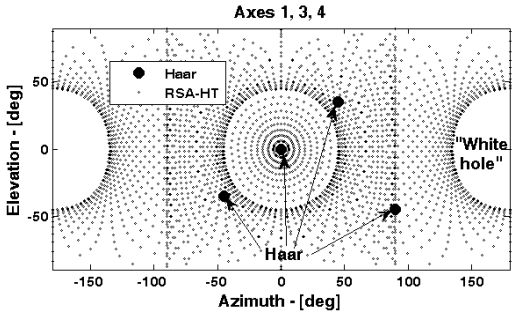

Fig. 3. Trace of RSA-HT BFs vector end projections on the spread of surface of one of the unit sphere3D projections

However, the difference between CRAIM-HT and CRAIMOT pictures is not so noticeable. This means that CRAIM-HT could be very useful for signal lossless compressing like CRAIMOT [8]. That is because of relative low percentage of "white holes" in comparison with the full area of US. If the signal vector-end targets in "white hole", the vector is not

coincidence with BF and we need a sum of weighted BFs to represent this signal. It decreases compression degree.

The best coverage of US (small areas of "white holes") can be achieved by the RA-HT, but acceptable is also the RSA-HT transform (approximately 60-70% coverage of US). This is slightly less than for CRAIM-HT (70-80%).

E. Signal Processing

In [8] we demonstrated that the CRAIMOT functions can be very useful for speech analysis, synthesis and compression. We expect that RA-HT functions are very perspective for the processing of pulse-like signals (edge detection [11], pulse filtering [12], image processing [13], and so on). We will come back to comprehensive discussions in the nearest future. At this moment, for a simple demonstration we picked out the sum of two CRAIM-HT BFs. The perfect reconstruction of this signal is also possible using the weighted sum of 15 Haar functions, but the average result can be achieved by 11-12 components. The reconstruction result is shown in Fig. 4.

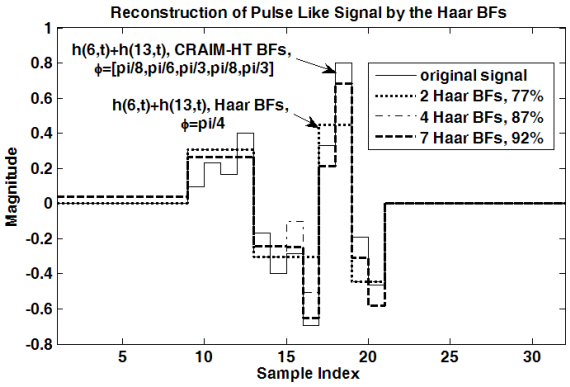

Fig. 4. Example of reconstruction of pulse-like signal by the Haar BFs

We see that the limited number of classical Haar functions does not allow to reconstruct the details of chosen signal even for 92% energy. This simple example shows also that the compression degree can be improved 6-7 times by the proper choice of transform for large number of shapes of pulse-like signals (because the diversity of RA-HT BFs shapes is infinite!).

III. FPGA Implementation of Analyzer-Synthesizer

This is the first trial of real implementation of RA-HT transform(s) into experimental devices. We expect that these devices will be used for prototyping other devices.

A. Development Environment

The used environment is the same as for the development of the CRAIMOT spectrum analyzer [9]. The *Altera's Quartus II v6.0* has been used as software design environment for the SANSYN module. The low-level design of the device is coded in VHDL. We implemented the SANSYN into *Altera's Cyclone II* FPGA. The *Altera's DSP Cyclone Development Kit* has been used to develop hardware for the current version of the analyzer-synthesizer. For the digital-to-analog conversion of spectrum/signal has been used the *Texas Instrument* DAC *TIDAC904E* (on the kit board). We performed visual control and capturing of DAC output signal using the *Tektronix TDS3054* oscilloscope. We used also *MATLAB Instrument Toolbox* facilities (*serial* object and related functions) to import captured shapes of signals/spectrum from *TDS3054* to MATLAB.

B. Architecture of the SANSYN Module

Generally, the SANSYN module (Fig. 5) contains the analyzer part and the synthesizer part. Both parts have a similar structure but not identical (see (1)). Two CORDIC blocks form the heart of the module. The input/output of analyzer/synthesizer (I/O register block) is organized as serial-to-parallel/parallel-to-serial registers (**s2p/p2s reg**) (see Fig. 6). Further, to save the space of this paper, we describe the analyzer part only.

1) Rotation Block

Fig. 6 presents a simplified block diagram of rotation block and I/O registers of the analyzer part of the SANSYN module. It corresponds with the second version of module (see next subsection), and it is the first half of the full module.

The core of analyzer/synthesizer is a rotation block that contains $n_C=2^{n-1}=N/2$ CORDIC cells. The rotation block includes also the accumulator (N words) to store the rotated vector. It also includes the angle vector register ($n\times N/2$ words) and the input/output buffer registers. The CORDIC cell performs the elementary Given's rotation and permutation of two samples:

$$\begin{bmatrix} y_m^j \\ y_{m+1}^j \end{bmatrix} = \begin{bmatrix} \sin(\varphi_j) & \cos(\varphi_j) \\ \cos(\varphi_j) & -\sin(\varphi_j) \end{bmatrix} \cdot \begin{bmatrix} x_m^j \\ x_{m+1}^j \end{bmatrix} \qquad (5)$$

where $m\in[1, N-1]$, but $j\in[1, n]$. Matrix (5) corresponds to the CRAIM-HT transform. We skip here more generalized expression for the RSA-HT and RA-HT transforms because of sophisticated indexing. The implemented version of CORDIC

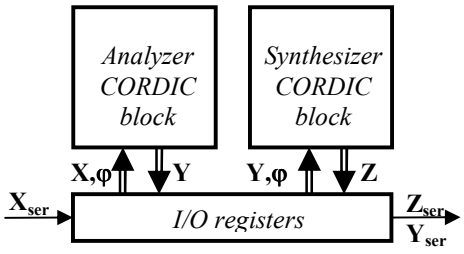

Fig. 5. Simplified structure of the RA-HT SANSYN module

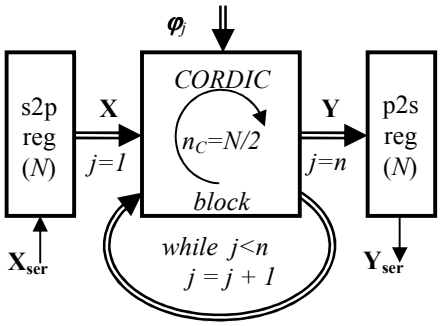

Fig. 6. Simplified block diagram of the RA-HT spectrum analyzer

block is capable of carrying out other RABOT transforms, for example, CRAIMOT. We keep notes for next papers. In the case of RA-HT transforms the CORDIC block performs some empty rotations due to zero angles (see (3)), in the second and the further phases of execution of transform. Here the potential is evident for optimization of the module in the nearest future.

2) Timing Diagram

When the analyzer has been started, the stream of samples ($\mathbf{X}_{ser}$ in Fig. 5 and Fig. 6, or **x_in** in Fig. 7) with the sample rate of clock **clk_out** (Fig. 7) fills the register **s2p reg** and the accumulator of CORDIC block. After incoming *N* samples the CORDIC block control counter (illustrated by the *while* loop in Fig. 6) has been initialized. The counter is driven by the clock with a period greater than T_{CORDIC} (>70 ns). When the counter reaches the end value *n* (the number of matrices **B**), the values of the spectrum vector **Y** (**y1_out, …, y8_out** in Fig. 7) are ready to be sent out. The output stream is sent out with the frequency of clock **clk_sp (**equal to the frequency of **clk_out**). The clock **clk_sp** has a suppression interval while rotations are performed. In such a way, if the spectrum calculation time does not exceed input sample time, we can send out output samples (spectrum) continuously in stream with a delay for N samples.

3) Signal Processing Unit

We plan to use the SANSYN module as the prototype of the main signal processing unit in the RA-HT based devices, to be described in following papers. One of them is submitted to this conference [12].

Theoretically, reader can imagine a device with structure like Fig. 5 where I/O block has been substituted by more sophisticated "black box".

C. Comparison of SANSYN Versions

We have several experimental versions of the SANSYN module. All of them are based on the CORDIC cells. Here we provide only a very brief description of the versions.

Basically, the first ("parallel") version of module code contains two VHDL *FOR* loops (we do not count an additional *FOR* loop necessary for the CORDIC cell code description). The inner loop organizes $N/2=2^{n-1}$ (4 in example (3)) CORDIC rotators in hardware (rotators correspond to rotations inside **B** matrix), but the outer loop is responsible for the change of matrices (execution phase). This version of SANSYN is the fastest but it consumes more hardware resources (see TABLE II). Besides, it has a relatively complicated pipelined structure and a low capability for modification.

In the second ("hybrid") version the *FOR* loop works akin the outer loop (the change of matrix **B**) in the "two-loops version". The implemented version uses 2^{n-1} simultaneously working rotation cells driven *n* times by the clock. We suggest that the second version is most perspective one for further development.

The third ("serial") version uses only one CORDIC rotator and it has a relatively complicated timing diagram and a low capability for modification .

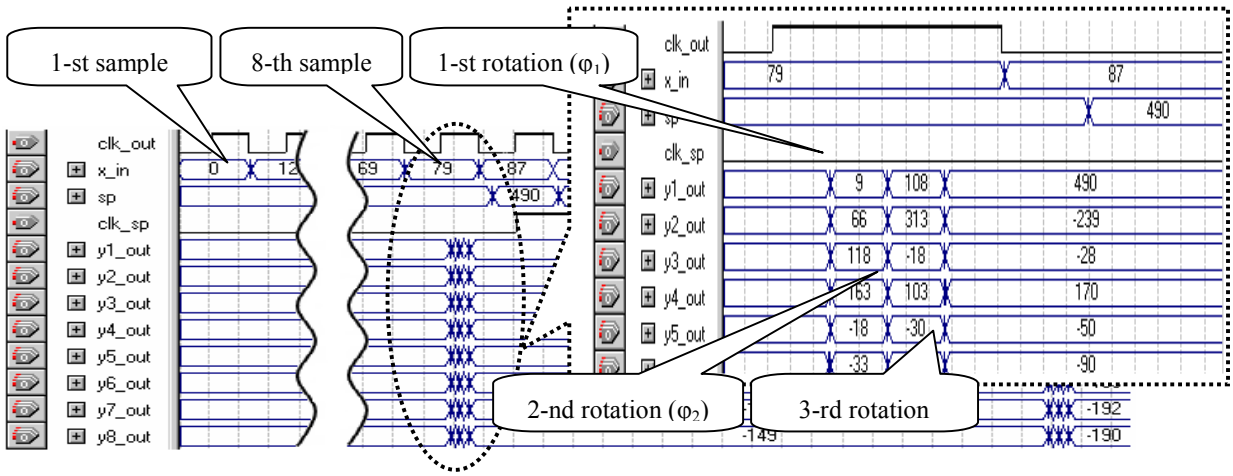

Fig. 7. Capture of the main timing diagrams of the CRAIM-HT analyzer version for N=8 in *Quartus II*

D. Parameters of Analyzer-synthesizer

The module is mostly VHDL coded. The core of module that corresponds to Fig. 5 contains approximately 700 VHDL strings. Additional service/control parts (I/O etc.) are coded in approximately 1000 VHDL strings.

The two tables above summarize some parameters of the

module and consumption of hardware resources. The speed of the implemented module depends on the speed of CORDIC cell. For the *Cyclone II EP2C35F672C6* chip the execution of 9-bits rotation requires approximately 70 ns. This time is practically independent of the clock because of the execution of rotation in hardware. The execution time has also a weak dependence on the number of simultaneous rotations.

We should remember also that the number of CORDIC cells and logic elements (in TABLE II) must be doubled for the module, on the whole. For example, for the module with $N=32$ we need ***2*(800+600*32/2)=20800*** logic cells. This means that the used *Cyclone II* chip allows the implementation of the full SANSYN module for $N_{max}=32$.

	FOR loops	*CORDIC cells*	*Logic Elements*	*Calculation Time (ns)*
1.	2	$n_C=n*2^{n-1}$	$\approx 800+600*n_C$	$\approx 70*n$, $(n\leq 3)$
2.	1	$n_C=2^{n-1}$	$\approx 800+600*n_C$	$\approx 70*n$
3.	0	$n_C=1$	$\approx 700+600*n_C$ $+50*n*2^{n-1}$	$\approx 70*n*2^{n-1}$

TABLE II
COMPARISON OF ANALYZER/SYNTHESIZER VERSIONS (F_{CLK}=100 MHz)

TABLE III
THE LIST OF PARAMETERS OF SANSYN

Parameter	*Value*
External clock used	f_c = 50 (100) MHz
Maximal number of angles	$n_\varphi=n*N/2$ = **5*16=80**
Maximal block length (samples)	$N = 2^n$= **32**
Wordlength for sample values	w = 10 bits, Q1.x FPA
CORDIC rotation time	T_{CORDIC}=70 ns
Sample (also processing) time	$T_s=n*T_{CORDIC}$

IV. CONCLUSIONS

- The present module is the first trial of practical implementation of RA-HT transform into FPGA. Three versions of SANSYN module are discussed. The device with parallel structure is the fastest but maximally consumes logic cells. The one-rotator device has a low speed. The module selected (with N/2 CORDIC rotators) for further development and implemented into *Cyclone II EP2C35F672C6* performs real-time spectrum analysis/signal synthesis for 32-sample block with sample stream 2.5 millions samples per second in time less than 400 ns.
- The SANSYN module will be used for the prototyping of RA-HT based devices. We consider this module as the main unit for perspective real-time pulse-like signal processing devices. First of all, we expect that such devices will be successfully used for the pulse-like signal compression, detection, and extraction, blurred edge detection in the image processing, and for other applications in acoustic and video signal processing. We continue to work on it.

ACKNOWLEDGMENT

We are greatly thankful to Andra Martinsone for collaboration and help. This work was supported in part by the Council of Science of Latvia under Grant 05.1654, the National Program "Modern Technologies in Telecommunications" and the ESF project “Support for the development of doctoral studies at Riga Technical University”.

REFERENCES

[1] P. Misans, "Introduction into the Haar like transforms based on rotation Angles." Scientific Proc. of Riga Technical University, Telecommunications and Electronics, Riga, RTU, vol. 7, Dec., 2007, pp. 6-13.
[2] http:\\www.ieee.org\ieeexplore
[3] M. Terauds, "Synthesis of discrete fast orthogonal transforms," the blueprint of Ph.D. dissertation, Faculty of Electronics and Telecommunications, Riga Technical University, to be published, 2008.
[4] P. Misans, M. Terauds, "Introduction into the fast orthogonal transforms based on rotation angles: A new methodical approach only or a gateway to novel DSP algorithms?," presented at the 5th Electronic Circuits and Systems Conference ECS'05, Bratislava, Slovakia on Sept. 8-9, 2005, in Conf. Proc., pp. 85-94.
[5] H. C. Andrews, "Multidimensional Rotations in Feature Selection," *IEEE Transactions On Computers*, Vol. 18, No. 5, pp. 1045-1051, Sept. 1971.
[6] P. Rieder et. al, “Parameterization and Implementation of Orthogonal Wavelet Transforms,” Available: *www.ieee.org\ieeexplore* 0-7803-3 192-3/96 1996 IEEE.
[7] P. P. Vaidyanathan, "A unified approach to orthogonal digital filters and wave digital filters, based on LBR two-pair extraction," *IEEE Transactions On Circuits And Systems*, Vol. CAS-32, No. 7, pp. 673-686, July 1985.
[8] G. Valters, P. Misans, "Initial version of FPGA-based CRAIMOT basis functions generator," presented at the 14th IEEE International Conference Mixed Design of Integrated Circuits and Systems MIXDES 2007, Ciechocinek, Poland, June 21-23, 2007, in Conf. Proc., pp. 632-637.
[9] P. Misans, G. Valters, "Initial version of FPGA-Based CRAIMOT spectrum analyzer," presented at the 6th Electronic Circuits and Systems Conference ECS'07, Bratislava, Slovakia, Sept. 6-7, 2007, in Conf. Proc. pp., 159-164.
[10] P. Misans, M. Terauds, G. Valters, U. Derums, N. Vasilevskis, "FPGA-Based CRAIMOT basis function generator," presented at the 25th IEEE Norchip Conference, Aalborg, Denmark, November 19-20, 2007, in Conf. Proc., 6 pages, ISBN 1-4244-1517-9/07/ IEEE, IEEE Catalog Number 07EX1896C.
[11] P. Misans, G. Valters, "Introduction into the parametrical Decomposition-Reconstruction filters based on Haar-like orthonormal transform," presented at the 6th Electronic Circuits and Systems Conference ECS'07, Bratislava, Slovakia, Sept. 6-7, 2007, in Proc. of ECS'07, pp. 107-112.
[12] P. Misans, G. Valters, M. Terauds, N. Vasilevskis, "Initial implementation of generalized Haar-like transforms into FPGA-Based devices – Part II: Decomposition Reconstruction filters," submitted to this proceeding 5 pages.
[13] P. Misans, U. Derums, "Introduction into the novel two-dimensional discrete orthogonal transforms based on rotation angles," presented at the 12th International Conference Electronics, May 18-20, Kaunas, Lithuania, paper (6 pp.) in press - in Proc. Electronics and Electrical Engineering, Kaunas: Technologija, 2008.